Molecular Systems Design & Engineering

Accepted Manuscript

This article can be cited before page numbers have been issued, to do this please use: A. P. Mártire, G. M. Segovia, O. Azzaroni, M. Rafti and W. A. Marmisollé, *Mol. Syst. Des. Eng.*, 2019, DOI: 10.1039/C9ME00007K.

ROYAL SOCIETY OF CHEMISTRY

rsc.li/molecular-engineering

View Article Online
DOI: 10.1039/C9ME00007K

Design, System, Application Statement

The oxygen reduction reaction (ORR) is one of the most important reactions in electrochemical energy converting systems. Among the different alternatives to overcome the limitation of using expensive Pt-based electrocatalysts, the use of conducting polymers have been proposed as ORR catalysts. However, this interesting alternative usually exhibits low efficiency, thus limiting the electrocatalytic applications of these macromolecular systems. Using layer-by-layer assembly, we were able to optimize the electrocatalytic properties of conducting polymer by synergistically combining them with O_2-absorbing metal-organic frameworks (MOFs). We demonstrate that rather than an electrocatalytic promotion effect caused by MOF metal sites available on the surface, the electrocatalytic enhancement arises from the selective uptake and preconcentration of oxygen in the MOF microporous matrix that ultimately acts as an oxygen reservoir linked to the polymeric electrocatalytic material. We believe that conducting polymers taken together with MOFs, as functional counterparts, represent a new synergy in materials science provided that they are able to offer an interfacial architecture exhibiting a more efficient response towards oxygen reduction. We consider that these results can lead to a new way of looking at conducting polymers as low-cost alternatives for ORR electrocatalysis as well as spark new research directions in electrochemical nanoarchitectonics.

View Article Online
DOI: 10.1039/C9ME00007K

Layer-by-Layer Integration of Conducting Polymers and Metal Organic Frameworks onto Electrode Surfaces: Enhancement of the Oxygen Reduction Reaction through Electrocatalytic Nanoarchitectonics

Ana Paula Mártire, Gustavo M. Segovia, Omar Azzaroni,* Matías Rafti,* and Waldemar Marmisollé*

Instituto de Investigaciones Fisicoquímicas Teóricas y Aplicadas (INIFTA), Departamento de Química, Facultad de Ciencias Exactas, Universidad Nacional de La Plata (UNLP), CONICET, (1900) La Plata, Argentina.

ABSTRACT

In this work we explore a nanoarchitectonics approach to construct functional composite nanomaterials with enhanced electrocatalytic properties. The functional electrodes were designed in order to combine two key elements: high surface area and porosity with electroactivity, thus enabling its application to the enhancement of the electrochemical oxygen reduction reaction (ORR). We propose a simple, yet unexplored, layer-by-layer (LbL) method which makes use of sequential assembly of colloidal suspensions of polyaniline/polystyrene sulfonate (Pani-PSS), and polyallylamine hydrochloride-coated ZIF-8 metal organic framework nanocrystals (PAH-ZIF-8). The Pani-PSS/PAH-ZIF-8 nanoarchitecture thus obtained benefits from the synergy between the electroactivity provided by negatively charged conducting polymer component (Pani-PSS), and the high-surface area porous environment provided by the positively charged MOF counterpart (PAH-ZIF-8). LbL-assembled films were found to be electrically connected and feature promising increases in the electrocatalytic currents obtained for the ORR in neutral pH aqueous environments.

* E-mail: azzaroni@inifta.unlp.edu.ar (O.A.)
E-mail: mrafti@quimica.unlp.edu.ar (M.R.)
E-mail: wmarmi@inifta.unlp.edu.ar (W.A.M.)

View Article Online
DOI: 10.1039/C9ME00007K

INTRODUCTION

Nanoarchitectures featuring the integration of different materials into structurally stable functional composites has become recently the focus of a multitude of research projects which tackled the problem from diverse perspectives due to the foreseen applications in diverse fields such as; e.g., energy storage and conversion, bio-nanotechnology, catalysis, and sensor technologies.[1–4] It is required for the feasibility of such practical applications that the actual assembly procedure does not present excessive complications, thus allowing for a reasonable trade-off between the degree of complexity and the enhanced functional properties obtained. This explains why it is so important to keep exploring methods and technologies for integrating molecular building blocks into well-defined organized assemblies. Research efforts on this matter are often referred to as "nanoarchitectonics", a term popularized by Ariga and co-workers.[1-4]

Poly-aniline (Pani) has been known for quite a long time, to be a cost-effective and very versatile conducting polymeric material.[5–7] Its integration into composites aiming to confer differential properties suitable for applications in electrocatalysis and energy has gained increasing attention from the scientific community.[8,9] In particular, integration of high-surface area porous materials such as Metal Organic Frameworks (MOFs) into the above mentioned composites offers the opportunity of creating suitable materials with an expanded range of possible uses.[10–12] MOFs are a relatively new family of microporous materials constituted by metal centers or metal clusters non-covalently bonded with organic multidentate linkers. Among its main features, MOFs present high surface areas, highly tailorable pore-wall chemistry, and the possibility of synthesis in relatively mild conditions to form either films or controlled size/shape nanostructures.[13–17] MOFs can endow films with ideal characteristics for electrochemical reactions (e.g., water splitting, CO_2 electroreduction), allowing for the coexistence of both, hydrophilic channels for the diffusion of charged species, and hydrophobic porosity needed for gas adsorption.[18–24]

In the last decade the concept of including MOFs into composites, or its use as precursors for the synthesis of electroactive materials for the Oxygen Reduction Reaction (ORR) was extensively explored, and many different strategies were followed.[25–29] Although it suffers from poor control over the morphologies obtained, calcination remains a popular approach; and the use of MOFs as templates for heteroatom-doped micro/mesoporous carbon features electrochemical promotion.[30–34] However, until very recently, conductive MOFs were not available and its integration into electrochemical platforms was conditioned to the presence of another component which will provide this fundamental

View Article Online
DOI: 10.1039/C9ME00007K

characteristic.[35–38] This view was radically changed by the recent work of Dincă et al.,[39–41] who introduced conductive MOFs, thus widening the palette of possible architectures and mechanisms for their use in electrocatalysis. Following these new paradigm MOF-nanosheets where showed to present considerable enhancement of the ORR.[42–44]

An alternative appealing approach for building functional nanomaterials is the use of layer-by-layer (LbL) technique, as it offers the possibility of self-limited and self-oriented growth. For this assembly to be feasible, it should include components capable of interact via either coulombic, van der Waals, Hydrogen bonding, or hydrophilic/hydrophobic interactions.[45–47] Although a vast majority of the LbL assemblies make use of polyelectrolytes,[48,49] there are examples in which layers were constructed using different nano-objects in order to create soft nanoarchitectures with tailored functional properties.[50,51] Hereby we explore a new design concept; i.e., the synthesis of LbL nanoarchitectures for the integration of high-surface area porous materials capable of incremented gas adsorption, embedded into a conductive electroactive matrix. In order to achieve this end, we first synthesized colloidal suspensions of both, Pani-PSS negatively charged electroactive polymer, and PAH-stabilized (Polyallylamine hydrochloride) positively charged colloidal suspensions of ZIF-8 MOF (a Zn-based archetypal Zeolitic Imidazolate microporous material, which was already shown to act as ORR enhancer).[20,52] ZIF-8 can be described as an infinite network of Zn^{2+} ions tetrahedrally coordinated with 2-methylimidazolate N-bidentate organic linkers, featuring high BET surface area (≈ 1500-1800 m^2 g^{-1}), and good resistance towards hydrolysis in moderate pH aqueous environments and ionic strengths.[53,54] We show for the first time that a LbL architecture is achievable using these pre-synthesized nanostructures; and moreover, that these films feature electrochemical activity and can act as enhancers of the neutral pH electrochemical ORR due to a synergetic effect between high surface-area porous material and electroactive conductive polymer, offering thus a cost-effective alternative to precious metal catalysts usually employed in energy conversion devices.

Experimental

Chemicals

Aniline, Ammonium Persulfate (APS), Poly (sodium 4-styrene sulfonate) (PSS) (Mw≈70kDa), Polyallylamine hydrochloride (PAH) (ca. 17.5 kDa), Polyethylenimine (PEI) (50% in H_2O, Mw ≈ 750kDa), $Zn(NO_3)_2.6H_2O$, and 2-methyl-imidazole (2m-Im) were purchased from Sigma-Aldrich. Methanol was obtained from Dorwil. Hydrochloric Acid and Potassium Chloride were purchased from Anedra. All solutions were prepared with Milli-Q water (18.2 MΩ cm).

View Article Online
DOI: 10.1039/C9ME00007K

FTIR Spectroscopy. Fourier transform infrared spectroscopy was performed using a using a FTIR Nicolet 480 spectrometer with a resolution of 1 cm^{-1}.

UV-Vis spectroscopy. The LbL assembly was built up on glass substrates for UV-visible measurements. Spectra were taken with an Agilent model 8453E diode array spectrophotometer.

DLS and Zeta Potential. Dynamic light scattering (DLS) measurements were carried out with a ZetaSizer Nano (Nano ZSizer-ZEN3600, Malvern, U.K.) at 25°C. The zeta potential was determined from the electrophoretic mobility measured by laser Doppler velocimetry using disposable capillary cells (DTS 1061 1070, Malvern) at 25°C with a drive cell voltage of 30 V and employing the monomodal analysis method.

Electrochemical measurements. Cyclic voltammetry was carried out with a Gamry Reference 600 potentiostat. A three-electrode Teflon-lined cell was used. The counter electrode used was a Pt wire and the reference electrode used was Ag/AgCl (3M NaCl) electrode. Gold electrodes were prepared by sputtering on glass plates.[55]

X-ray diffraction (XRD). Calculated X-ray diffraction patterns were obtained from Cambridge Crystallographic Data Base (CCDB) ZIF-8 files using Mercury® software.[56] Diffraction experiments on the synthesized materials were recorded at room temperature under ambient conditions on a Phillips X'Pert-1 apparatus.

Electron Microscopy. Transmission Electron Microscopy (TEM) images were obtained with a JEM 1200 EX II (JEOL Ltd.) equipped with a digital camera Erlangshen ES1000W, model 785 (Gatan Inc.). The samples were observed under an accelerating voltage of 100 kV.

Pani-PSS synthesis

Firstly, a 5 mM aniline in 5 mM (in monomer units) PSS solution in 0.5 M HCl was stirred for 15 minutes. Then, solid APS was added to reach a 5 mM concentration and the solution was stirred overnight at room temperature, yielding a dark green suspension. After synthesis, the solution was neutralized by adding 10% KOH up to pH 7. This stock colloidal dispersion remained stable for months.

Synthesis of ZIF-8 colloidal suspensions and modification with PAH

Stock ZIF-8 dispersions were obtained by mixing equal volumes of 50 mM $Zn(NO_3)_2.6H_2O$ and 25 mM 2m-Im methanolic solutions at room temperature, to yield a stoichiometric final molar ratio. After

View Article Online
DOI: 10.1039/C9ME00007K

40 minutes reaction time, a cloudy colloidal dispersion of ZIF-8 was obtained. The procedure to obtain colloidal dispersions later used for the LbL assembly was the following; 15 mL of the methanolic stock ZIF-8 colloidal suspensions were added to 135 mL of 0.022 mg mL^{-1} PAH 5 mM KCl aqueous solution. The final concentration results in 2.5 mM Zn^{2+} and 0.02 mg mL^{-1} PAH with (methanol: water) volume ratio equal to (1:9). This colloidal dispersion was characterized by DLS and employed for the LbL assembly (see below).

View Article Online
DOI: 10.1039/C9ME00007K

Results and Discussion

Pani-PSS complexes were characterized by DLS, showing a single size distribution with a maximum at 25 nm (volume distribution), whereas the zeta potential determined in the as-synthesized pH 7 stock solution was -25 mV (**Fig. 1**). ZIF-8 and PAH-ZIF-8 colloidal suspensions were characterized using DLS and TEM. Although freshly prepared ZIF-8 suspensions were found to have already a positive Z-potential (**Fig. 1**), colloidal modified with PAH coating showed a marked Z-potential increase with no significant size modification.

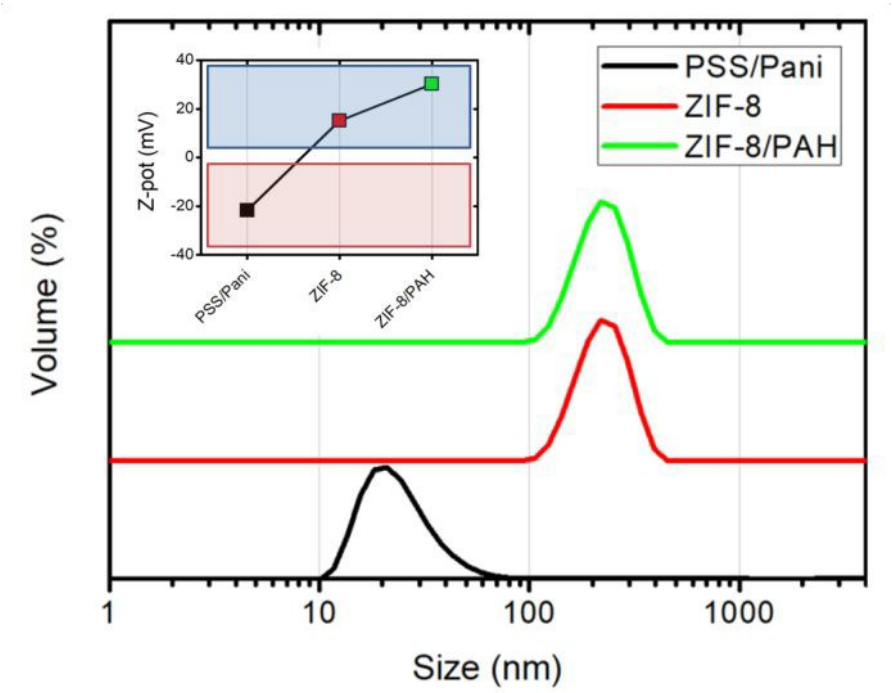

Figure 1. Volume averaged DLS and Z-potential determinations of the colloidal suspensions used for the LbL assembly.

Formation of Aggregates

After the colloidal characterization of the individual building blocks, the possibility of electrostatically-driven assembly was explored by directly producing aggregates from the stable aqueous suspensions. Pani-PSS/PAH-ZIF-8 aggregates were prepared by adding 2 mL of Pani-PSS stock colloidal suspension to a 100 mL volume of PAH-ZIF-8 fresh colloid. The solution immediately became blue and flocks appeared. This dispersion was kept under magnetic stirring for 2 hours. Then, the flocks were collected by centrifuging at 6500 rpm for 10 minutes. Finally, the solid was dried overnight at 60°C. This powder was then characterized by FTIR and XRD.

View Article Online
DOI: 10.1039/C9ME00007K

Vibrational spectroscopy characterization of the building blocks and the aggregates was performed by FTIR in the transmission mode by dispersing the solid components into KBr pellets (**Fig. 2**). The spectrum of the aggregates of Pani-PSS/PAH-ZIF-8 reveals its composite nature as several bands of the individual components can be clearly assigned. The presence of the PSS can be shown by a band at 825 cm^{-1}, assigned to the out-of-plane aromatic CH deformation, and a band at 1007 cm^{-1} that has been assigned to in-place aromatic CH bending.[57,58] Moreover, the presence of the sulfonate group is revealed by a band at 1035 cm^{-1} assigned to a symmetric stretching[57,59] and doublet at about 1121 and 1171 cm^{-1}, assigned to the asymmetric stretching of the $–SO_3^-$ group.[57] On the other hand, many of the main bands of ZIF-8 are also present in the aggregates.[60,61] Particularly, the band at 1420 cm^{-1} can be attributed to the imidazole ring stretching mode, whereas the bands at 1179, 1146 and 995 cm^{-1} are associated to in-plane ring bending and those appearing at 1310, 950 and 760 cm^{-1} correspond to out-of-plane imidazole bending modes.

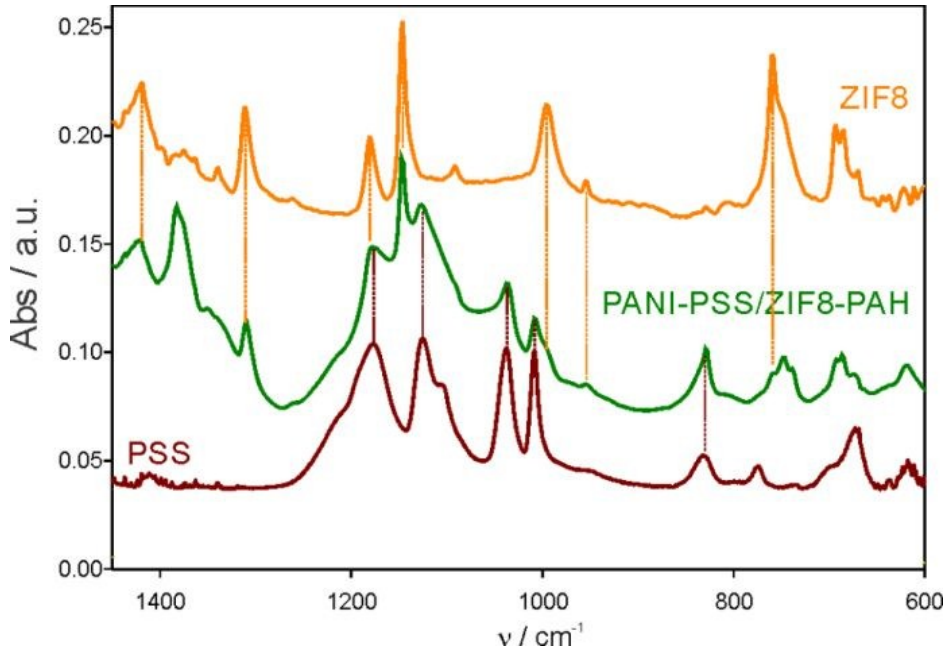

Figure 2. FTIR spectra of ZIF-8, PSS, and Pani-PSS/PAH-ZIF-8 aggregates.

Structural determination of films was carried via X-ray diffraction indirectly on the aggregates formed under identical conditions in order to obtain films with a thickness enough for detection. As can be observed in **Fig. 3**, there is a good agreement between the calculated diffractogram using reported ZIF-8 structure and the obtained results for the aggregates.

View Article Online
DOI: 10.1039/C9ME00007K

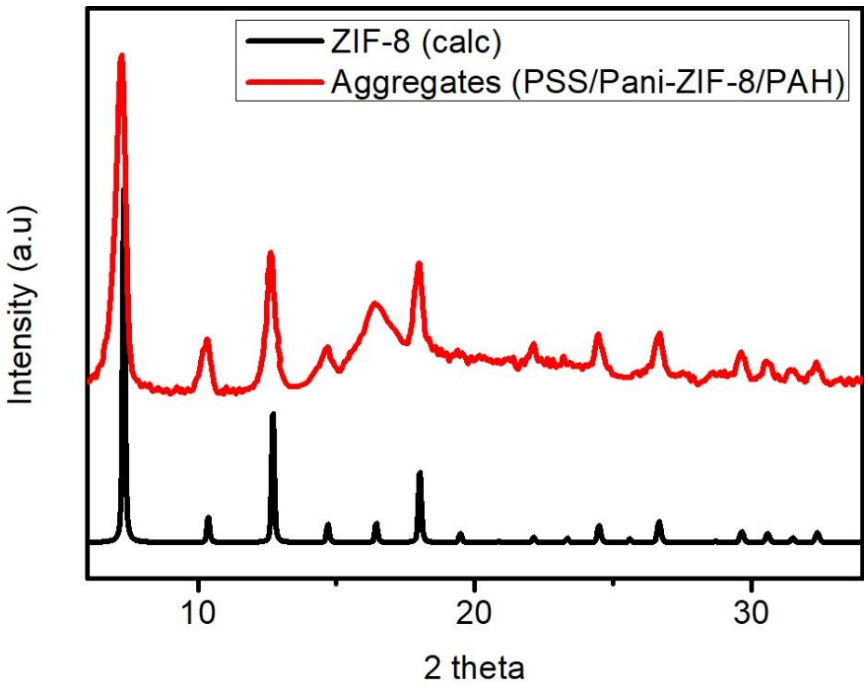

Figure 3. Comparison of calculated ZIF-8, and Pani-PSS/PAH-ZIF-8 aggregates.

Layer-by-layer assembly

The LbL assembly was started by immersing the substrates in a 1 mg mL^{-1} PEI solution for 10 minutes.[52] After that, the substrates were washed with DI water for 5 minutes. Then, the substrates were alternatively dipped in a Pani-PSS and PAH-ZIF-8 (or PAH) colloidal suspensions for 15 minutes with a washing step in DI water before the next growth step (**Scheme 1**). **Fig. 4** shows the absorbance at 680 nm of LbL-modified glass substrates after different number of deposition cycles. The increment of the absorbance indicates the effective growing up of the composite film, which is probably driven by the electrostatic interactions between the charged building blocks. Integration of Pani-PSS and PAH-ZIF-8 building blocks in the LbL assembly was confirmed by XPS (**see ESI**). The spectrum of 1-bilayer-modified gold electrode presents peaks consistent with the presence of both Pani-PSS and PAH-ZIF-8, as revealed by comparison with the XPS spectra of the individual blocks.

The successful electrostatic assembly was further confirmed by QCM experiments in which the mass increment due to each LbL step was determined together with its mass composition ratio r = m(Pani-PSS)/m(ZIF-8-PAH)=0.81 (**see ESI**.).

View Article Online
DOI: 10.1039/C9ME00007K

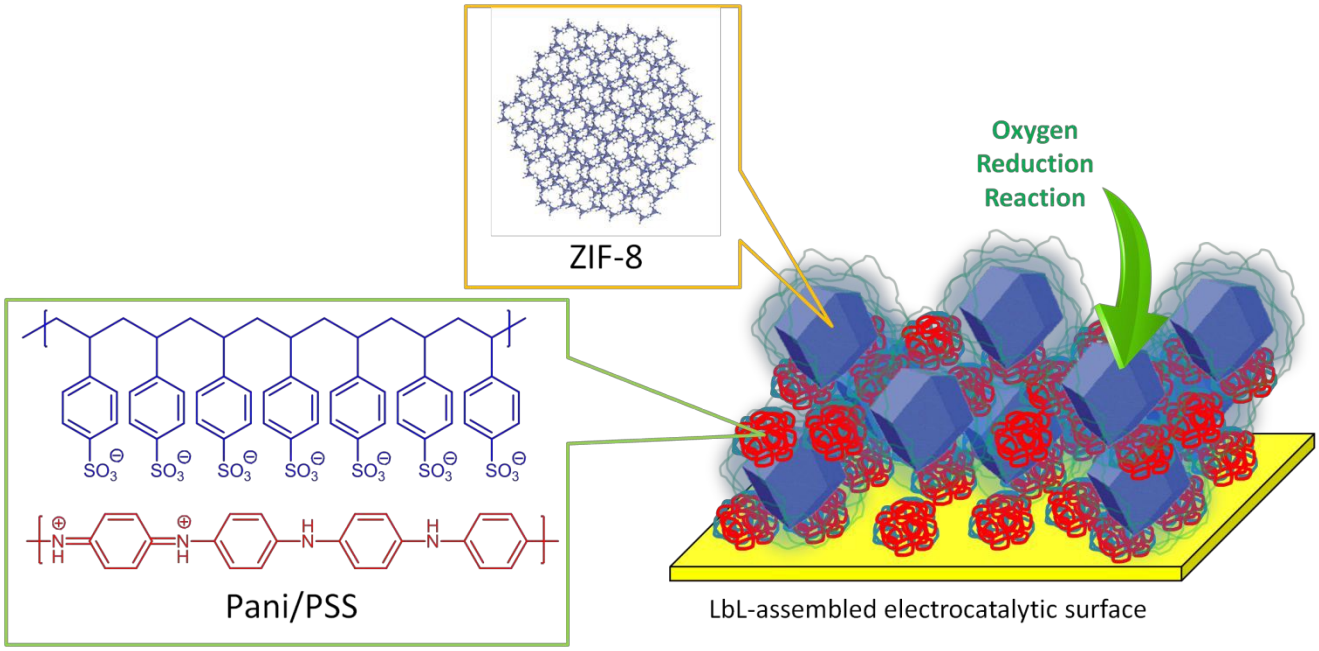

Scheme 1. Cartoon describing the hybrid electrocatalytic interface constituted of LbL-assembled Pani-PSS and PAH-ZIF-8.

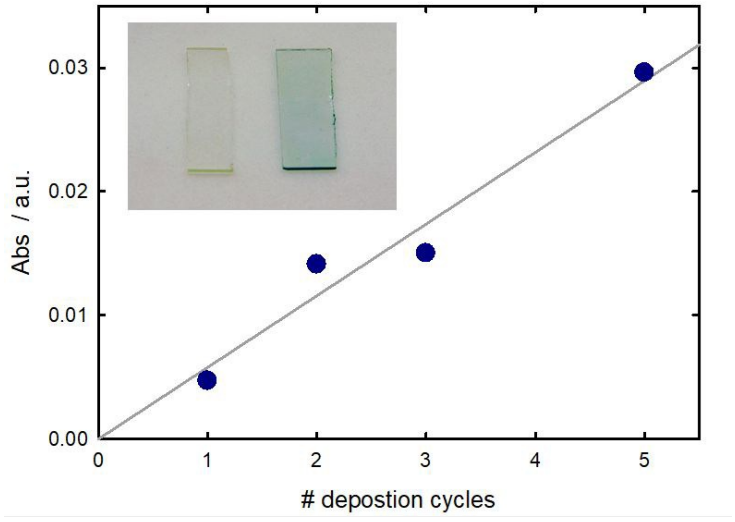

Figure 4. Absorbance at 680 nm of LbL-modified glass substrates as a function of the number of deposition cycles. Inset: digital images of the glass plate before and after 5 cycles of deposition.

TEM characterization of ZIF-8 MOF obtained from methanolic synthesis and after functionalization with PAH and combination with Pani-PSS can be observed in **Fig. 5**. LbL assemblies were grown on TEM grids in order to obtain in-situ imaging of conducting polymer-embedded MOF nanocrystals.

View Article Online
DOI: 10.1039/C9ME00007K

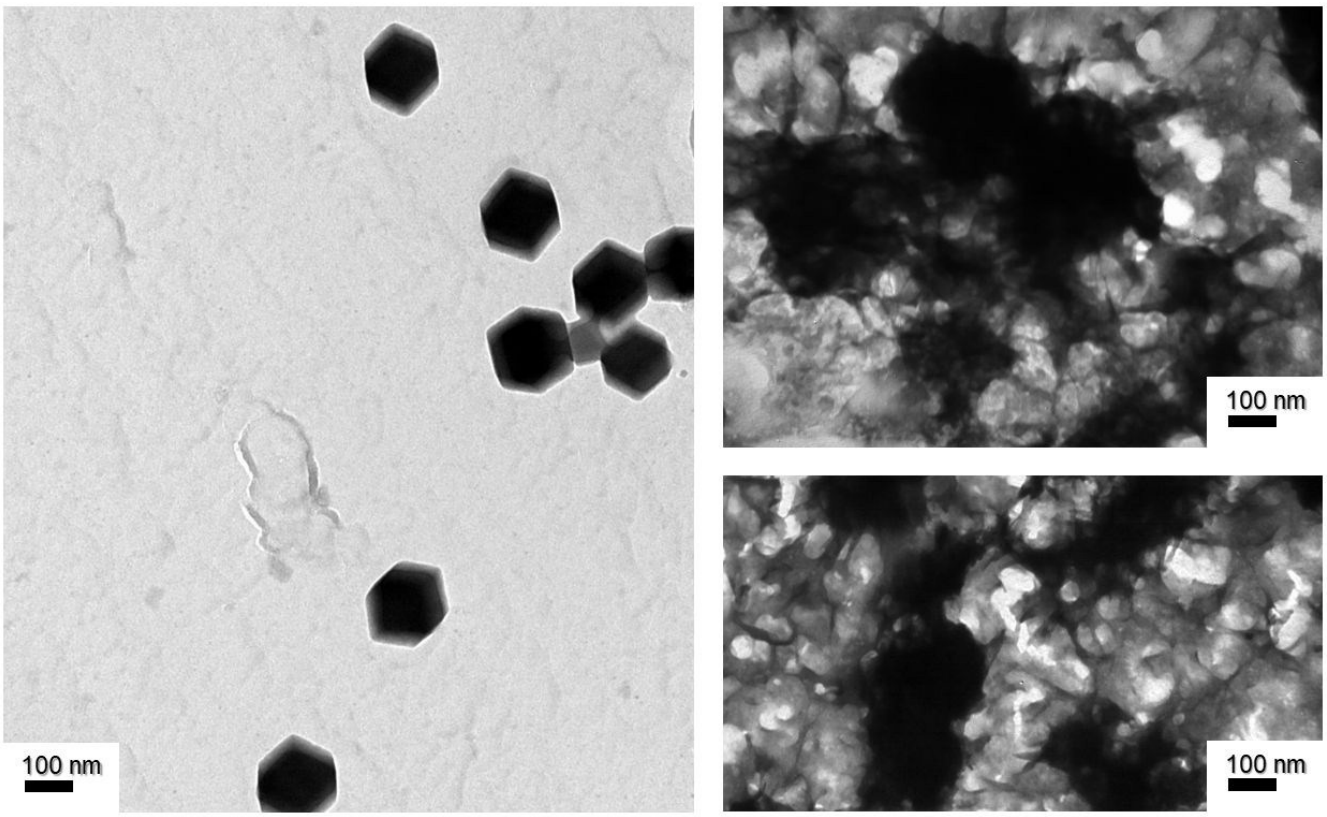

Figure 5. TEM images showing the as-synthesized ZIF-8 nanocrystals used as building blocks, and (right) two different fields of view in which the LbL assembly was carried over PEI-modified TEM copper grids.

Electrochemical behavior of the LbL assemblies

The electrochemical response of the LbL assembled films deposited on Au electrodes previously functionalized with PEI was studied by cyclic voltammetry in neutral solutions. Although Pani in not electroactive at neutral aqueous electrolytes, the Pani-PSS complex is expected to retain the electroactivity when increasing the pH owing to the doping effect of the negatively charged sulfonate groups.[62,63] As shown in **Fig. 6**, the voltammetric response of the Pani-PSS containing films show a pair of peaks at about 0.1V corresponding to the first redox transition in Pani from the completely reduced state (leucoemeraldine) to the oxidized (emeraldine).[64] In acidic conditions this redox couple appears as higher potentials, with more defined shapes; but as the pH increases, this couple shifts to lower potentials and the voltammetric peaks become broader. In the case of Pani films, a loss of conductivity and electroactivity is observed when pH is increased above ca. 4, leading to the degradation of the electrochemical degradation of the polymer.[65] In the present case, the response was

View Article Online
DOI: 10.1039/C9ME00007K

stable and no degradation effects were observed after continuous cycling in this solution, proving the increased electroactivity by the PSS effect.

Moreover, the increment of the integrated voltammetric charge of these pair of peaks is indicative of the amount of electrochemically active material deposited after each functionalization cycle. A linear dependence of this charge on the number of functionalization cycles was obtained (inset in **Fig. 6**). This correlation indicates that the electroactive component integrated in the LbL assembly is electrochemically connected within the films, which is not necessarily valid for all the LbL assemblies with non-electroactive counterparts.[55] Thus, it is possible the functional integration of the electroactive block in the composite films by this simple nanoarchitectonic approach.

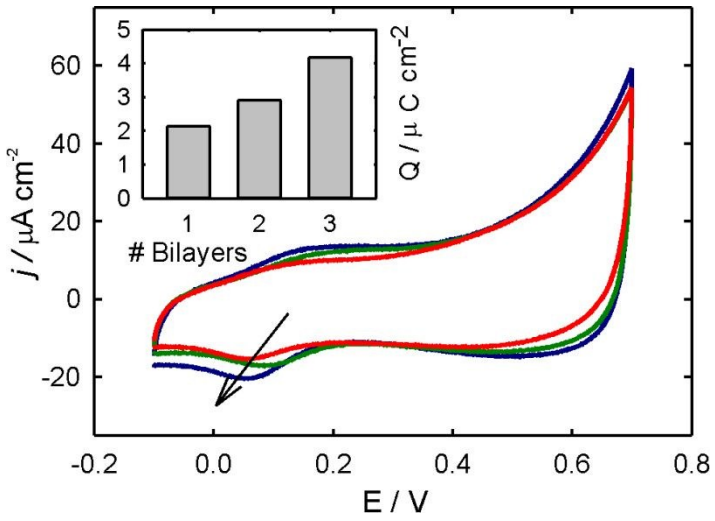

Figure 6. Voltammetric response of the LbL assemblies of Au/PEI/Pani-PSS/(PAH-ZIF-8/Pani-PSS)$_n$ (n=0 red, n=1 green, n=2 blue), at v=0.2 Vs^{-1} in 0.1 M KCl. Integrated voltammetric charges of the cathodic peak of the conducting polymer at about 0.1 V as a function of the number of Pani-PSS layers is depicted in the inset.

Then, the evaluation was focus on the functional response of the MOFs integrated within the films. As previously demonstrated, the integration of ZIF-8 on electrosynthesized conducting polymers yields an increment of the ORR current as a consequence on the local preconcentration of O_2 in the MOF material. Thus, to evaluate the enhancement of the ORR current by the presence of the ZIF-8 nanocrystals, cyclic voltammetry in air-saturated solutions after different functionalization steps was performed between 0.5 and -0.6V (**Fig. 7**). For comparison, the voltammetric results for the assembly with PAH without ZIF-8 was also carried out. By analysing the cathodic current after different

View Article Online
DOI: 10.1039/C9ME00007K

deposition steps for both assemblies, it is possible to conclude that the incorporation of ZIF-8 nanocrystals leads to an enhancement of the ORR, whereas it is reduced in the assembly without the MOF. In order to quantify this effect, the integrated charge of the ORR voltammetric wave was computed as a function of the functionalization steps. These values are presented in **Fig. 8**, where an increment of the ORR after depositing any ZIF-8 containing layer is observed. Moreover, the charge due to the ORR increases as the amount of the deposited material increases. These results prove the functional integration of the ZIF-8 nanocrystals by the LbL approach. In contrast, control experiments performed on the films produced by bulk casting of the aggregates formed by direct mixture of Pani-PSS and PAH-ZIF-8 dispersions a less efficient electrocatalytic behaviour in terms of the ORR performance **(see ESI)**, thus suggesting that the LbL integration approach becomes essential for optimizing the functional properties of the nanocomposite material in terms of the electrocatalytic response.

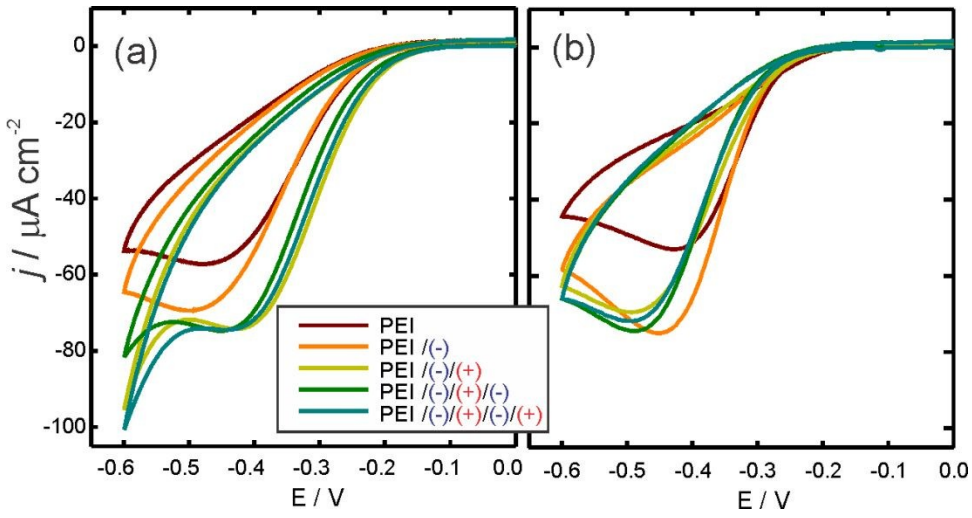

Figure 7. Cyclic voltammograms at 10 mV s^{-1} in the ORR region in air-saturated 0.1 M KCl solution of Au electrodes after different stages of functionalization of the LbL assemblies: **(a)** Pani-PSS (-) / PAH-ZIF-8 (+); **(b)** Pani-PSS (-) / PAH (+).

A direct comparison between our results and previous results from the literature is not trivial. The main reason is that most of previous results on the oxygen reduction reaction on conducting polymer electrodes were performed in either acidic or alkaline media, whereas our experiments were performed in neutral conditions. In this regard, Kumar and Chen[66] reported the electrocatalytic reduction of oxygen at conducting polymer-modified glassy carbon electrodes under neutral conditions. These authors reported an oxygen electroreduction current density of 28 μA/cm^2 at 0.6 V. Taking as a reference point these results from Kumar and Ashok, we observe that our LbL nanoarchitected

View Article Online
DOI: 10.1039/C9ME00007K

electrodes exhibit a better electrocatalytic efficiency provided that under the same polarization conditions they reach values display larger electrocatalytic currents, 100 μA/cm^2.

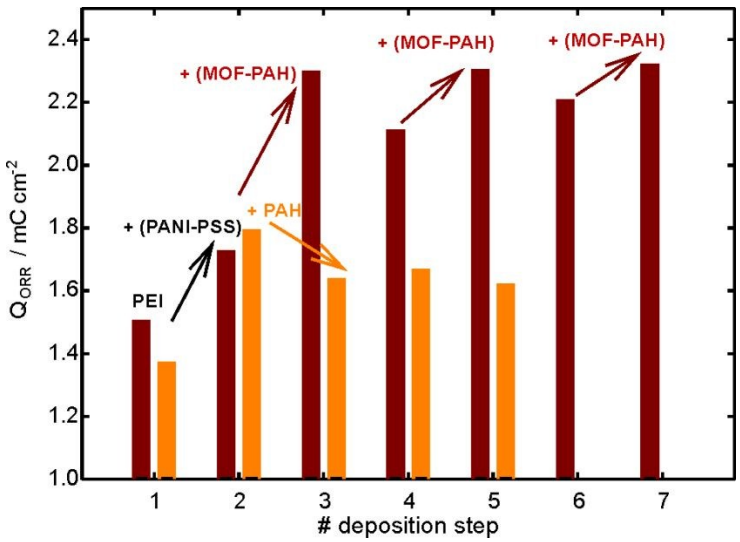

Figure 8. Integrated charge of the cathodic waves for different functionalization stages in Fig. 7.

Conclusions

The spontaneous, layer-by-layer self-assembly of conducting polymer-MOF particle nanostructured films, reported here, exemplifies well our proposed nanoarchitectonic approach to advanced electrocatalytic electrodes surfaces. This work demonstrates the viability to fabricate Pani-PSS)/ ZIF-8 MOF nanocrystals (PAH-ZIF-8) composite thin films via layer-by-layer assembly for ORR electrocatalysis. The purpose of this study was to demonstrate that the synergy between the electroactivity provided by Pani and the high surface area and porosity of ZIF-8 MOF nanocrystals is a key element to obtain nanocomposite electrode surfaces with enhanced ORR characteristics. Considering the simplicity of our approach, combined with the electrocatalytic properties found for LbL electrodes, we believe we have demonstrated a potent alternative in fabricating MOF-based electrocatalytic surfaces. Currently, we are exploring and fine-tuning critical features, such as improved electron transfer properties and optimized MOF loading, within LbL nanoconstructs.

Acknowledgments

View Article Online
DOI: 10.1039/C9ME00007K

The authors acknowledge financial support from ANPCyT (PICT-2015-0239, PICT-2016-1680), Universidad Nacional de La Plata (PPID-X016). M.R., W.M., and O.A. are CONICET staff members. G.M.S. holds a doctoral scholarship from CONICET. Technical support by M. Lorena Cortez and Desire Di Silvio from CiC-BiomaGune (Spain) is gratefully acknowledged.

References

1 M. Aono and K. Ariga, *Adv. Mater.*, 2016, **28**, 989–992.

2 J. Kim, J. H. Kim and K. Ariga, *Joule*, 2017, **1**, 739–768.

3 K. Ariga and M. Aono, in *Materials Nanoarchitectonics*, Wiley-VCH Verlag GmbH & Co. KGaA, Weinheim, Germany, 2018, pp. 1–6.

4 W. Qi and J. Yan, in *Materials Nanoarchitectonics*, Wiley-VCH Verlag GmbH & Co. KGaA, Weinheim, Germany, 2018, pp. 141–154.

5 D. L. Raffa and F. Battaglini, *J. Electroanal. Chem.*, 2001, **504**, 120–124.

6 X. Lei, X. Guo, L. Zhang, Y. Wang and Z. Su, *J. Appl. Polym. Sci.*, 2007, **103**, 140–147.

7 X. Shi, A. L. Briseno, R. J. Sanedrin and F. Zhou, *Macromolecules*, 2003, **36**, 4093–4098.

8 G. E. Fenoy, B. Van der Schueren, J. Scotto, F. Boulmedais, M. R. Ceolín, S. Bégin-Colin, D. Bégin, W. A. Marmisollé and O. Azzaroni, *Electrochim. Acta*, 2018, **283**, 1178–1187.

9 N. Ashok Kumar and J. B. Baek, *Chem. Commun.*, 2014, **50**, 6298–6308.

10 S. Yuan, L. Feng, K. Wang, J. Pang, M. Bosch, C. Lollar, Y. Sun, J. Qin, X. Yang, P. Zhang, Q. Wang, L. Zou, Y. Zhang, L. Zhang, Y. Fang, J. Li and H. C. Zhou, *Adv. Mater.*, 2018, **1704303**, 1–35.

11 T. Kitao, Y. Zhang, S. Kitagawa, B. Wang and T. Uemura, *Chem. Soc. Rev.*, 2017, **46**, 3108–3133.

12 D. Sheberla, J. C. Bachman, J. S. Elias, C.-J. Sun, Y. Shao-Horn and M. Dincă, *Nat. Mater.*, 2017, **16**, 220–224.

13 L. E. Kreno, K. Leong, O. K. Farha, M. Allendorf, R. P. Van Duyne and J. T. Hupp, *Chem. Rev.*, 2012, **112**, 1105–1125.

14 T. R. Cook, Y. R. Zheng and P. J. Stang, *Chem. Rev.*, 2013, **113**, 734–777.

15 Q. Yang, Q. Xu and H. L. Jiang, *Chem. Soc. Rev.*, 2017, **46**, 4774–4808.

View Article Online
DOI: 10.1039/C9ME00007K

16 O. M. Yaghi, M. O'Keeffe, N. W. Ockwig, H. K. Chae, M. Eddaoudi and J. Kim, *Nature*, 2003, **423**, 705–714.

17 C. H. Hendon, A. J. Rieth, M. D. Korzyński and M. Dincă, *ACS Cent. Sci.*, 2017, **3**, 554–563.

18 J. S. Tuninetti, M. Rafti, A. Andrieu-Brunsen and O. Azzaroni, *Microporous Mesoporous Mater.*, 2016, **220**, 253–257.

19 M. Jahan, Q. Bao and K. P. Loh, *J. Am. Chem. Soc.*, 2012, **134**, 6707–6713.

20 M. Rafti, W. A. Marmisollé and O. Azzaroni, *Adv. Mater. Interfaces*, 2016, **3**, 1600047.

21 N. Kornienko, Y. Zhao, C. S. Kley, C. Zhu, D. Kim, S. Lin, C. J. Chang, O. M. Yaghi and P. Yang, *J. Am. Chem. Soc.*, 2015, **137**, 14129–14135.

22 D. Micheroni, G. Lan and W. Lin, *J. Am. Chem. Soc.*, 2018, **140**, 15591–15595.

23 D.-H. Nam, O. S. Bushuyev, J. Li, P. De Luna, A. Seifitokaldani, C.-T. Dinh, F. P. García de Arquer, Y. Wang, Z. Liang, A. H. Proppe, C. S. Tan, P. Todorović, O. Shekhah, C. M. Gabardo, J. W. Jo, J. Choi, M.-J. Choi, S.-W. Baek, J. Kim, D. Sinton, S. O. Kelley, M. Eddaoudi and E. H. Sargent, *J. Am. Chem. Soc.*, 2018, **140**, 11378–11386.

24 M. P. Suh, H. J. Park, T. K. Prasad and D.-W. Lim, *Chem. Rev.*, 2012, **112**, 782–835.

25 M. Shao, Q. Chang, J.-P. Dodelet and R. Chenitz, *Chem. Rev.*, 2016, **116**, 3594–3657.

26 Y. Nie, L. Li and Z. Wei, *Chem. Soc. Rev.*, 2015, **44**, 2168–2201.

27 M. Khalid, A. M. B. Honorato, H. Varela and L. Dai, *Nano Energy*, 2018, **45**, 127–135.

28 C. A. Downes and S. C. Marinescu, *ChemSusChem*, 2017, **10**, 4374–4392.

29 M. D. Allendorf, A. Schwartzberg, V. Stavila and A. A. Talin, *Chem. - A Eur. J.*, 2011, **17**, 11372–11388.

30 K. Shen, X. Chen, J. Chen and Y. Li, *ACS Catal.*, 2016, **6**, 5887–5903.

31 H. Zhong, J. Wang, Y. Y. Zhang, W. Xu, W. Xing, D. Xu, Y. Y. Zhang and X. Zhang, *Angew. Chemie Int. Ed.*, 2014, **53**, 14235–14239.

32 Q. Lai, Y. Zhao, Y. Liang, J. He and J. Chen, *Adv. Funct. Mater.*, 2016, **26**, 8334–8344.

33 J. Tong, W. Li, L. Bo, J. Ma, T. Li, Y. Li, Q. Zhang and H. Fan, *ACS Sustain. Chem. Eng.*, 2018, **6**, 8383–8391.

View Article Online
DOI: 10.1039/C9ME00007K

34 J. Tang and Y. Yamauchi, *Nat. Chem.*, 2016, **8**, 638–639.

35 C. H. Hendon, D. Tiana and A. Walsh, *Phys. Chem. Chem. Phys.*, 2012, **14**, 13120–13132.

36 V. Stavila, A. A. Talin and M. D. Allendorf, *Chem. Soc. Rev.*, 2014, **43**, 5994–6010.

37 J. Liu, T. Wächter, A. Irmler, P. G. Weidler, H. Gliemann, F. Pauly, V. Mugnaini, M. Zharnikov and C. Wöll, *ACS Appl. Mater. Interfaces*, 2015, **7**, 9824–9830.

38 L. Wang, X. Feng, L. Ren, Q. Piao, J. Zhong, Y. Wang, H. Li, Y. Chen and B. Wang, *J. Am. Chem. Soc.*, 2015, **137**, 4920–4923.

39 L. Sun, M. G. Campbell and M. Dincă, *Angew. Chemie Int. Ed.*, 2016, **55**, 3566–3579.

40 T. C. Narayan, T. Miyakai, S. Seki and M. Dincă, *J. Am. Chem. Soc.*, 2012, **134**, 12932–12935.

41 D. Sheberla, L. Sun, M. A. Blood-Forsythe, S. Er, C. R. Wade, C. K. Brozek, A. Aspuru-Guzik and M. Dincă, *J. Am. Chem. Soc.*, 2014, **136**, 8859–8862.

42 S. Zhao, Y. Wang, J. Dong, C.-T. He, H. Yin, P. An, K. Zhao, X. Zhang, C. Gao, L. Zhang, J. Lv, J. Wang, J. Zhang, A. M. Khattak, N. A. Khan, Z. Wei, J. Zhang, S. Liu, H. Zhao and Z. Tang, *Nat. Energy*, 2016, **1**, 16184.

43 Y. Xu, B. Li, S. Zheng, P. Wu, J. Zhan, H. Xue, Q. Xu and H. Pang, *J. Mater. Chem. A*, 2018, **6**, 22070–22076.

44 G. Hai, X. Jia, K. Zhang, X. Liu, Z. Wu and G. Wang, *Nano Energy*, 2018, **44**, 345–352.

45 T. Lee, S. H. Min, M. Gu, Y. K. Jung, W. Lee, J. U. Lee, D. G. Seong and B.-S. Kim, *Chem. Mater.*, 2015, **27**, 3785–3796.

46 L. L. Del Mercato, P. Rivera-Gil, A. Z. Abbasi, M. Ochs, C. Ganas, I. Zins, C. Sönnichsen and W. J. Parak, *Nanoscale*, 2010, **2**, 458–467.

47 W. Knoll and R. C. Advincula, *Functional Polymer Films*, Wiley-VCH Verlag GmbH & Co. KGaA, Weinheim, Germany, 2011.

48 R. R. Costa and J. F. Mano, *Chem. Soc. Rev.*, 2014, **43**, 3453–3479.

49 E. Tjipto, J. F. Quinn and F. Caruso, *Langmuir*, 2005, **21**, 8785–8792.

50 K. Ariga, Y. Yamauchi, G. Rydzek, Q. Ji, Y. Yonamine, K. C.-W. Wu and J. P. Hill, *Chem. Lett.*, 2014, **43**, 36–68.

View Article Online
DOI: 10.1039/C9ME00007K

51 Q. Ji, S. B. Yoon, J. P. Hill, A. Vinu, J.-S. Yu and K. Ariga, *J. Am. Chem. Soc.*, 2009, **131**, 4220–4221.

52 G. E. Fenoy, E. Maza, E. Zelaya, W. A. Marmisollé and O. Azzaroni, *Appl. Surf. Sci.*, 2017, **416**, 24–32.

53 B. Wang, A. P. Côté, H. Furukawa, M. O'Keeffe and O. M. Yaghi, *Nature*, 2008, **453**, 207–211.

54 J. A. Allegretto, J. Dostalek, M. Rafti, B. Menges, O. Azzaroni and W. Knoll, *J. Phys. Chem. A*, 2018, acs.jpca.8b09610.

55 W. A. Marmisollé, E. Maza, S. Moya and O. Azzaroni, *Electrochim. Acta*, 2016, **210**, 435–444.

56 I. J. Bruno, J. C. Cole, P. R. Edgington, M. Kessler, C. F. Macrae, P. McCabe, J. Pearson and R. Taylor, *Acta Crystallogr. Sect. B Struct. Sci.*, 2002, **58**, 389–397.

57 R. A. Weiss, A. Sen, C. L. Willis and L. A. Pottick, *Polymer (Guildf).*, 1991, **32**, 1867–1874.

58 D. Krishnamurti and R. Somashekar, *Mol. Cryst. Liq. Cryst.*, 1981, **65**, 3–22.

59 C. R. Martins, G. Ruggeri and M. A. De Paoli, *J. Braz. Chem. Soc.*, 2003, **14**, 797–802.

60 K. S. Park, Z. Ni, A. P. Cote, J. Y. Choi, R. Huang, F. J. Uribe-Romo, H. K. Chae, M. O'Keeffe and O. M. Yaghi, *Proc. Natl. Acad. Sci.*, 2006, **103**, 10186–10191.

61 G. Lu and J. T. Hupp, *J. Am. Chem. Soc.*, 2010, **132**, 7832–7833.

62 A. M. Bonastre, M. Sosna and P. N. Bartlett, *Phys. Chem. Chem. Phys.*, 2011, **13**, 5365–5372.

63 P. A. Kilmartin, A. Martinez and P. N. Bartlett, *Curr. Appl. Phys.*, 2008, **8**, 320–323.

64 P. . Bartlett and E. N. . Wallace, *J. Electroanal. Chem.*, 2000, **486**, 23–31.

65 J. Scotto, M. I. Florit and D. Posadas, *J. Electroanal. Chem.*, 2018, **817**, 160–166.

66. S. A. Kumar, S.-M. Chen, *Journal of Molecular Catalysis A: Chemical*, 2007, **278**, 244–250.

View Article Online
DOI: 10.1039/C9ME00007K

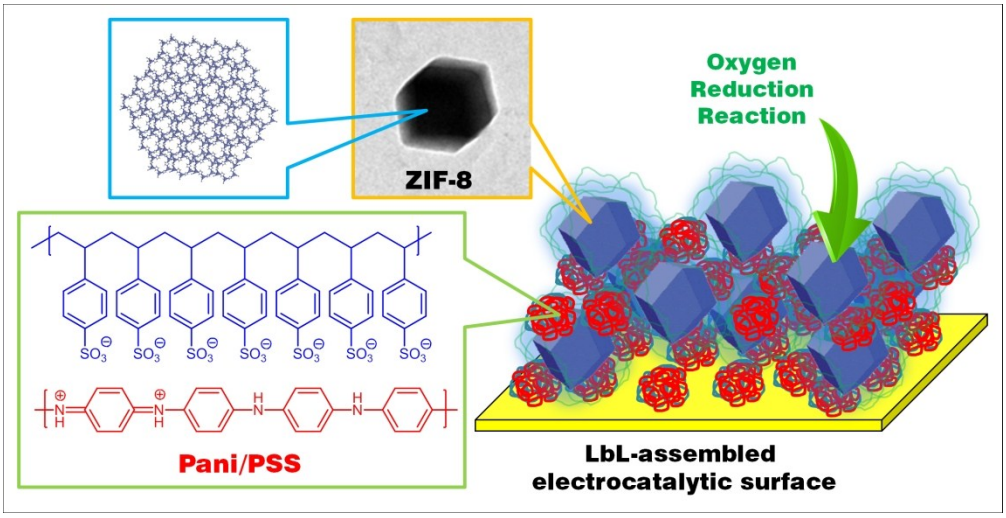

Table of Contents graphic

394x200mm (150 x 150 DPI)